Prediction of the Three-Dimensional Turbulent Flow in Stirred Tanks

Suzanne M. Kresta and Philip E. Wood
Dept. of Chemical Engineering, McMaster University, Hamilton, Ontario, Canada, L8S 4L7

Efforts to model the turbulent flow in stirred tanks require accurate boundary conditions at the tip of the impeller, not just of velocities, but of the turbulence quantities k and ϵ. Kolar's (1982) phenomenological, swirling radial jet model of the impeller region is extended by using a two-equation $k-\epsilon$ turbulence model to obtain direct estimates of k and ϵ on the impeller periphery. The model is extended and clarified, so that the number of parameters required for its application is reduced to two: the rotational speed and the diameter of the impeller. Three-dimensional simulations allow a realistic treatment of the baffles. Agreement of the modeling results with recently published experimental data is excellent. This is particularly true in the important impeller discharge zone, where details of the predicted behavior of the turbulence kinetic energy and dissipation rate are in quantitative agreement with the available data. Based on these results, average values of ϵ are calculated, along with the zones over which they apply. For the impeller discharge zone, the dimensionless, volume-averaged ϵ is 0.19.

Introduction

Stirred tanks are widely used in the chemical industry for mixing of single and multiphase fluids. Studies of the fluid flow characteristics have received wide attention due to design requirements such as scale-up criteria. Attention has typically been focused on integrated dimensionless quantities such as N_p, the power number, and N_q, the flow number. However, not much progress can be made in understanding the mixing mechanism in these tanks, especially for multiphase systems, without a better understanding of the detailed hydrodynamics within the vessel. In particular, models that describe the drop size distribution in a liquid-liquid dispersion, or models that describe mixing in chemical reactors, require estimates of the eddy sizes. The size of the eddies is directly related to local levels of the turbulence kinetic energy and its dissipation rate. The quantity of current experimental work on this flow field (Mahouast et al., 1989; Wu and Patterson, 1989; Ranade and Joshi, 1989, Ranade et al., 1989; Stoots and Calabrese, 1989) gives an indication of the importance of the problem.

Mathematical modeling of a fundamental kind in which conservation equations are solved subject to initial and boundary equations can provide detailed information about the flow field that would be very difficult to obtain experimentally. This has been attempted by Harvey and Greaves (1982a, b), Placek and Tavlarides (1985), Placek et al. (1986), Ju et al. (1987, 1990), and Kaminoyama et al. (1988). Progress in this area has been difficult, however, due to a shortage of experimental information on higher order turbulence quantities, which has only recently become available. These are needed not only to build the mathematical models, but also to validate them.

In this study a two-equation ($k-\epsilon$) turbulence model is used to investigate the turbulent flow field in a stirred tank agitated by a Rushton-style disk turbine. This same $k-\epsilon$ model has been used by several authors previously to study the flow patterns within stirred tanks (Placek and Tavlarides, 1982; Harvey and Greaves, 1982a, b; Middleton et al., 1986; Ju et al. 1987, 1990; Pericleous and Patel, 1987; Kaminyama et al., 1988; Hutchings et al., 1989). It is crucial to the model predictions that accurate boundary conditions be applied and it is clear from these earlier papers than an appropriate set of boundary conditions, especially with respect to turbulence modeling, has not yet been established for the agitator zone. This problem is similar to the $k-\epsilon$ model predictions of the complicated flow patterns that exist in the swirl combustor.

Correspondence concerning this paper should be addressed to P. E. Wood.

With different boundary conditions at the combustor inlet, the predicted flow field in the combustor can change dramatically from no recirculation zone to a toroidal recirculating vortex at the center of the combustor (Ramos, 1984); hence it is clear that accurate boundary conditions are required to give accurate predictions of the flow field in the bulk.

The boundary conditions near the impeller blades, which characterize the highly inhomogeneous turbulence generated by the impeller, have been studied quite extensively. Experimental observations (Van't Riet and Smith, 1975; Yianneskis et al. 1987; Stoots and Calabrese, 1989) suggest that the flow generated by the passing turbine blades consists mainly of trailing vortices that are being continuously shed. Velocity measurements at a single point in the impeller stream show a strong periodic component with superimposed fluctuations. One model for the impeller discharge stream was put forward by Placek and Tavlarides (1985). This is a mechanistic model based on the trailing vortex concept initially proposed by Van't Riet and Smith (1975), which is capable of providing estimates of the turbulence energy, k_p, of the large-scale vortices in the impeller discharge stream. The model cannot, however, be used to provide estimates of the turbulence dissipation rate ϵ, which is also required near the impeller blades. Furthermore, it is the average values of the velocities and turbulence quantities that are required as input to the $k-\epsilon$ model, so it is not likely that dynamic modeling of the vortices being shed from the impeller is required. These dynamic predictions must be averaged in some sense to obtain useful boundary conditions. On the average, the flow generated by the turbine is jetlike. Because the impeller is rotating, this jet is not purely radial but also has a swirl, or tangential component. The concept of using a tangential jet as a model to simulate the impeller discharge flow has been proposed by several authors (DeSouza and Pike, 1972; Obeid et al., 1982). Ju et al. (1987, 1990) compute the flow field using the tangential jet boundary condition, which requires knowledge of three experimental parameters and assumes a zero gradient of k and ϵ at the impeller periphery. They concentrate their comparisons on the velocity field in the bulk of the tank, where agreement with experimental results is good. Agreement of the model results with the turbulence quantities k and ϵ, however, is qualitative at best (Ju et al., 1987). The weaknesses of the tangential jet model are discussed by Kolar et al. (1984), who developed the more general swirling radial jet (SRJ) model to obtain outlet velocity profiles. Unfortunately, these models cannot give any information about the turbulence characteristics near the impeller blades, and it is this information that is required as input for a $k-\epsilon$ model simulation for the turbulence in the entire tank.

Extension of impeller zone modeling to provide reliable predictions of k and ϵ at the impeller periphery is crucial to progress. It has been shown experimentally that the mean velocity field in the impeller discharge stream has a similarity profile that is established only a very short distance from the impeller. In particular, the observed velocity field is the same as that which would be produced by a turbulent, swirling radial jet. Velocity profiles predicted by Kolar et al. (1984) using this idealization show very good agreement with experimental data; however, problems in this early version of the SRJ model resulted in a number of parameters of unclear physical significance. In this paper, the SRJ model is further developed and clarified, so that the only parameters required for its application are the peak discharge velocity and flow angle at the impeller tip. Based on the detailed experimental results available in this region, optimum parameters are suggested that require only the rotational speed and diameter of the impeller as input. Instead of the mixing length hypothesis used by Kolar et al. (1984), the $k-\epsilon$ model is used to close the governing equations, and to quantify the turbulence characteristics. One of the major objectives of this paper is to extend the phenomenological, swirling radial jet model of the impeller region (Kolar et al., 1982) by using a $k-\epsilon$ turbulence model to obtain direct estimates of k and ϵ on the impeller periphery.

Modeling of this flow field is further complicated by the addition of baffles around the tank wall. These baffles encourage top to bottom circulation in the tank, but also make the flow field three dimensional over part of the volume, and introduce a drag that makes it difficult to represent the flow realistically as an axisymmetric (two-dimensional) one, especially with regard to the turbulence quantities k and ϵ. Harvey and Greaves (1982a) and Pericleous and Patel (1987) model the effects of the baffles by introducing a pressure-induced drag term in the θ component of the equations of motion. This drag term contains a coefficient that is, in essence, a tuning parameter. Chen and Wood (1988) found that, for the SRJ boundary condition, if this parameter is set to zero an incorrect velocity field results. The most reasonable predictions were obtained when it was set to 10^{-5}. For the boundary conditions used by Harvey and Greaves (1982a), the best value for the parameter was 1. Placek and Tavlarides (1982, 1985), Placek et al. (1986), and Ju et al. (1987, 1990) model the stirred tank by introducing modifications to the turbulence model and boundary conditions, which meets with limited success. Hutchings et al. (1989) deal with the baffles by complete suppression of the tangential velocity in the axisymmetric case, and its suppression in the baffle region for the three-dimensional case. It was found that while this irrotational treatment results in reasonable mean velocity profiles, it has severe implications for the prediction of turbulence quantities, resulting in differences of up to three orders of magnitude from a full three-dimensional, swirling case. In this work, the baffles are not modeled but are included as part of the three-dimensional calculation domain. This has allowed reproduction of details of the flow field around the baffles as they are observed in flow visualization experiments, and very good prediction of the turbulence quantities. This approach also requires much less *a priori* knowledge of the flow field than previous methods.

Turbulence Model

The reported simulations consist of two parts:

1. Solution of the SRJ model to obtain the boundary conditions at the tip of the impeller as described by Wood and Chen (1985)
2. Three-dimensional simulations of the flow using FLUENT, a commercial software package

The two-equation ($k-\epsilon$) model is used in both parts of this study because it is the most tested and reliable turbulence model available. Although it will not give the amount of information that a mean Reynolds stress model will give, it requires an order of magnitude less computation time and gives predictions of the mean velocities that are of comparable accuracy to the higher order models. The model constants used are given in Table 1.

Table 1. $k-\epsilon$ Model Constants Used in Simulations

Simulation	C_μ	$C_{\epsilon 1}$	$C_{\epsilon 2}$	σ_ϵ	σ_k
SRJ model	0.09	1.43	1.92	1.3	1.0
FLUENT	0.09	1.44	1.92	1.3	1.0

Swirling Radial Jet Model of Impeller Discharge Flow

It has been known for some time that the turbulent stream ejected from a Rushton turbine behaves like a tangential jet (DeSouza and Pike, 1972), and subsequently this model was modified to the more general case of a swirling radial jet (Kolar et al., 1984). In the analysis presented by Kolar et al. (1982, 1984) the mixing length hypothesis was used to close the mean momentum equations and solutions were obtained for the radial component of the mean velocity profile. The results were in good agreement when compared to the radial velocity data for several different types of radial impellers. This suggests that the basic model is a good one for predicting the mean velocity in the impeller stream. However, this type of closure gives no information whatever about the turbulence kinetic energy and its dissipation rate in the vicinity of the impeller blades. If the $k-\epsilon$ model is to be used to predict the turbulence quantities in the tank, then profiles of k and ϵ are needed along every boundary surface. The approach used here is to apply the model of the swirling radial jet to predict profiles of both the mean velocity and turbulence quantities along the periphery of the volume swept out by the impeller. The standard $k-\epsilon$ model subject to the boundary layer and high Reynolds number approximations is used to establish boundary conditions. The same model, in its unsimplified form, is used for tank simulations.

Reduction and transformation of governing equations

The radial turbulent jet with swirl is governed by the mean equations of motion and the continuity equation. A cylindrical coordinate system was selected, with its origin at the center of the impeller. At steady state, the momentum and continuity equations, subject to the assumptions of high Reynolds number and the boundary layer approximation, reduce to:

$$\frac{\partial(rV_r)}{\partial r}+\frac{\partial(rV_z)}{\partial z}=0 \tag{1}$$

$$V_r\frac{\partial V_r}{\partial r}+V_z\frac{\partial V_r}{\partial z}-\frac{V_\theta^2}{r}=\frac{1}{\rho}\frac{\partial \tau_{rz}}{\partial z} \tag{2}$$

$$V_r\frac{\partial V_\theta}{\partial r}+V_z\frac{\partial V_\theta}{\partial z}+\frac{V_rV_\theta}{r}=\frac{1}{\rho}\frac{\partial \tau_{\theta z}}{\partial z} \tag{3}$$

A standard $k-\epsilon$ model (Launder and Spalding, 1972) is used to close this set of equations. The constitutive equations for the turbulent fluxes are given by:

$$\tau_{rz}=-\rho\overline{v_r'v_z'}=\rho\nu_t\frac{\partial V_r}{\partial z} \tag{4}$$

$$\tau_{\theta z}=-\rho\overline{v_\theta'v_z'}=\rho\nu_t\frac{\partial V_\theta}{\partial z} \tag{5}$$

With the eddy viscosity defined by:

$$\nu_t=0.09\frac{k^2}{\epsilon} \tag{6}$$

The governing transport equations for k and ϵ, subject to the boundary layer approximation are:

$$V_r\frac{\partial k}{\partial r}+V_z\frac{\partial k}{\partial z}=\frac{\partial}{\partial z}\left(\frac{\nu_t}{\sigma_k}\frac{\partial k}{\partial z}\right)+B-\epsilon \tag{7}$$

$$V_r\frac{\partial \epsilon}{\partial r}+V_z\frac{\partial \epsilon}{\partial z}=\frac{\partial}{\partial z}\left(\frac{\nu_t}{\sigma_\epsilon}\frac{\partial \epsilon}{\partial z}\right)+\frac{\epsilon}{k}\left[C_{\epsilon 1}B-C_{\epsilon 2}\epsilon\right] \tag{8}$$

$$B=\nu_t\left(\frac{\partial V_z}{\partial z}\right)^2+\nu_t\left(\frac{\partial V_\theta}{\partial z}\right)^2 \tag{9}$$

The momentum integrals that express the conservation of radial momentum and angular momentum may be written:

$$\lim_{r\to\infty}\int_{-\infty}^{\infty}\rho rV_r^2dz=M_\infty \tag{10}$$

$$\int_{-\infty}^{\infty}\rho r^2V_rV_\theta dz=G \tag{11}$$

This gives a total of four governing equations, two momentum integral constraints, and two constitutive equations, plus continuity, in three dimensions. Solution of these differential equations would be a difficult task. By performing a coordinate transformation $(r, \theta, z) \rightarrow (r, \xi)$, the problem can be substantially reduced. This transformation is depicted graphically in Figure 1, where r and θ are the radial and azimuthal directions, and ξ is the direction of flow in the impeller discharge. From Figure 1, the following observations can be made:

1. The angle β is exactly 90° at the circle of radius e, where ξ is equal to zero; this is the origin of the system of tangential half planes

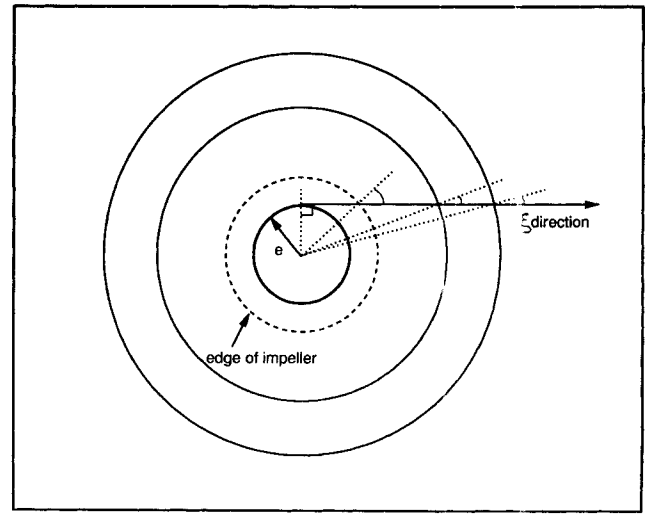

Figure 1. Graphical depiction of coordinate tranformation $(r, \theta, z) \rightarrow (r, \xi)$

2. The angle β decreases as r increases, going to zero as $r \to \infty$.

3. At any radial position, given the angle of declination of the flow from the purely radial direction, e can be determined from

$$\sin \beta = \frac{e}{r} \quad \text{or} \quad \cos \beta = \frac{\xi}{r} \tag{12}$$

4. The position of the impeller periphery relative to e is thus fully determined by the flow angle β_o at the periphery, or at any other radial position where the SRJ model holds. For a given impeller diameter, a single measurement of the flow angle allows e to be determined explicitly.

5.

$$\xi = \sqrt{r^2 - e^2} \tag{13}$$

Following Riley (1962) and Kolar et al. (1982), the flow field in this system of tangential half-planes can be expressed by the following geometrical relations:

$$V_r = q\frac{\xi}{r} \qquad V_\theta = q\frac{e}{r} \tag{14}$$

$$\tau_{rz} = \tau_{\xi z}\frac{\xi}{r} \qquad \tau_{\theta z} = \tau_{\xi z}\frac{e}{r} \tag{15}$$

where q is the velocity component in the ξ direction, and $\tau_{\xi z}$ is the turbulent shear stress in the ξ direction.

Using the transformation $(r, \theta, z) \rightarrow (\xi, z)$, the governing equations (Eqs. 1-11), for the SRJ become:

$$\frac{\partial}{\partial \xi}(\xi q) + \frac{\partial}{\partial z}(\xi V_z) = 0 \tag{16}$$

$$q\frac{\partial q}{\partial \xi} + V_z\frac{\partial q}{\partial z} = \frac{1}{\rho}\frac{\partial \tau_{\xi z}}{\partial z} \tag{17}$$

$$q\frac{\partial k}{\partial \xi} + V_z\frac{\partial k}{\partial z} = \frac{\partial}{\partial z}\left(\frac{\nu_t}{\sigma_k}\frac{\partial k}{\partial z}\right) + \frac{\tau_{\xi z}}{\rho}\frac{\partial q}{\partial z} - \epsilon \tag{18}$$

$$q\frac{\partial \epsilon}{\partial \xi} + V_z\frac{\partial \epsilon}{\partial z} = \frac{\partial}{\partial z}\left(\frac{\nu_t}{\sigma_\epsilon}\frac{\partial \epsilon}{\partial z}\right) + \frac{\epsilon}{k}\left[c_{\epsilon_1}\frac{\tau_{\xi z}}{\rho}\frac{\partial q}{\partial z} - c_{\epsilon_2}\epsilon\right] \tag{19}$$

Table 2. Similarity Profiles as a Function of η, Determined Using k - ϵ Model

η	q'	$g(\eta)$	$f(\eta)$	$p(\eta)$	$m(\eta)$
0.0	1.000	0.000	0.000	0.158	0.061
0.1	0.978	0.016	0.590	0.159	0.061
0.2	0.915	0.030	1.153	0.160	0.061
0.3	0.821	0.039	1.670	0.158	0.061
0.4	0.707	0.043	2.124	0.150	0.057
0.5	0.582	0.041	2.507	0.136	0.051
0.6	0.454	0.036	2.815	0.114	0.042
0.7	0.327	0.028	3.047	0.088	0.031
0.8	0.204	0.018	3.204	0.057	0.019
0.9	0.088	0.008	3.291	0.026	0.008
1.0	0.000	0.000	3.310	0.000	0.000

$\lambda = 0.16838$

The constitutive equations collapse to:

$$\tau_{\xi z} = \rho \nu_t \frac{\partial q}{\partial z} \tag{20}$$

and the momentum integral constraints reduce to:

$$J = \int_{-\infty}^{+\infty} q^2 \xi \, dz = M_\infty = \frac{G}{e} \tag{21}$$

This transformed set of equations expresses the impeller stream turbulent flow field in the system of half-planes tangential to the cylinder of radius e. The cylinder axis is coincident with the axis of the jet symmetry.

Similarity solution and resulting profiles

On closer examination, it becomes apparent that these equations have exactly the same form as those defining the turbulent radial jet with no swirl studied by Wood and Chen (1985). These equations admit a similarity solution, with similarity length and velocity scales defined as:

$$\delta(\xi) = \lambda \xi \quad \text{and} \quad q_M(\xi) = \frac{\gamma}{\xi} \tag{22}$$

respectively. The stream function is defined by:

$$q = \frac{1}{\xi}\frac{\partial \Psi}{\partial z} \quad \text{and} \quad V_z = -\frac{1}{\xi}\frac{\partial \Psi}{\partial z} \tag{23}$$

and the dimensionless similarity functions are:

$$\eta = \frac{z}{\delta(\xi)} \tag{24}$$

$$f(\eta) = \frac{\Psi}{q_M(\xi)\delta(\xi)\xi} \tag{25}$$

$$g(\eta) = \frac{\overline{v_\xi' v_z'}}{q_M^2(\xi)} \tag{26}$$

$$p(\eta) = \frac{k}{q_M^2(\xi)} \tag{27}$$

$$m(\eta) = \frac{\epsilon}{q_M^3(\xi)/\delta(\xi)} \tag{28}$$

Using these transformations and variable definitions, the coupled set of partial differential equations, Eqs. 16-20, can be reduced to a coupled set of ordinary differential equations in the single similarity variable η. This set of ordinary differential equations has boundary conditions at the jet centerline and jet edge, and can be solved using the calculation procedure described by Wood (1978) and Wood and Chen (1985) to yield the similarity profiles of f, g, p, and m. The similarity profiles are untransformed to obtain the stream function, Reynolds stress k, and ϵ, respectively, all as functions of η. The computed values of the similarity variables are given at a series of points in Table 2.

There are two important things that must be considered due to the nature of this solution, both intimately related to the jet width. The first concerns the value of λ, the second relates to the virtual origin of the jet.

The jet spreading rate, or λ, is in fact not a variable in these equations. It is an eigenvalue that is determined in the course of the problem solution. This is a direct consequence of the fact that the equations are singular in form, due to the complete neglect of molecular diffusion in their formulation. The locus of the singularity is at $z = \delta(\xi)$, which defines the jet width. This means that at the jet boundary, the profiles will not just approach zero, but will be identically equal to zero. This mathematical limitation will allow some simplifications in the development of predictions of e and β_o.

The lack of freedom in specification of λ leads to an apparent contradiction between the definition of $\delta(\xi)$ and the value of λ. Experimental results lead to the conclusion that the jet width is equal, or nearly equal to, the blade width at the impeller boundary. The origin of ξ is fully specified by the direction of flow at the impeller boundary. This leads to an overspecified problem. In the similarity length scale at the impeller tip, all three variables are fixed. This conflict is resolved by realizing that the similarity equations are invariant to the transformation $(\xi) \rightarrow (\xi + \xi_v)$. This allows specification of the jet width at the impeller periphery without violation of the previously defined origin of the coordinate ξ. The virtual origin, ξ, and the jet geometry are depicted in Figure 2.

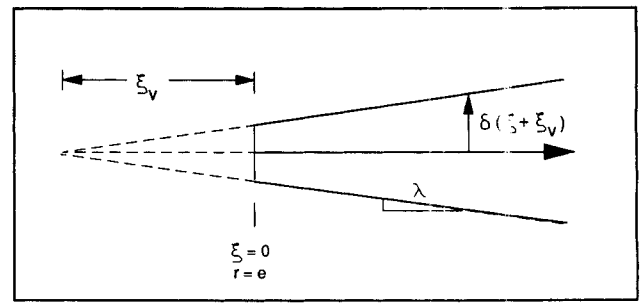

Figure 2. Jet geometry illustrating virtual origin.

$$e=\frac{G}{M_\infty}=\frac{G}{J}$$

Since the objective is to define the boundary conditions at the impeller tip, the values required for deconvolution should be defined as close to that point as possible. Consideration of experimental evidence, as shown in Table 3 and Figure 3, leads to adoption of the values

$$q_{M,o}=V_{TIP}=\pi ND$$
$$\beta_o=45° \qquad (29)$$
$$\delta_o=\frac{D}{10}$$

Although the value of $q_{M,o}$, averaged over all cited experimental results, is $1.18V_{TIP}$, the median is $1.05V_{TIP}$. The median is more useful in this case because it minimizes the influence of faulty data. The jet width δ_o is set equal to the half-blade width. This means that there may be some underprediction of the velocities close to the edges of the blade; but from Figure 3 this deviation is still within the range of the experimental results. Note that these results span a period of twenty years,

Experimental and theoretical predictions of e and β

Deconvolution of the similarity variables f, p, and m into the SRJ variables, q, V_z, k, and ϵ requires knowledge of γ, λ (calculated as part of the solution), $\delta(\xi)$, and $q_M(\xi)$. Further deconvolution of q into V_r and V_θ requires the use of e. As stated earlier, e can be defined in two ways: by the declination of flow (β) at any radial position where the SRJ model holds, or through the equality

Table 3. Experimental Data for Maximum Velocity and Flow Angle at Impeller Tip

Source	Instrument*	C	$2r/D$	$\frac{V_{r,m}}{\pi ND}$	β	$\frac{V_{\theta,m}}{\pi ND}$	$\frac{q_m}{\pi ND}$
Keller (1985)	LDA	T/3	1.18	0.55	—	—	—
Armstrong & Ruszkowski (1988)	LDA	T/3	1.02	0.74	—	—	—
Wong & Huang (1988)	HFA	T/2, T/3	1.2	0.68	40	—	(0.888)
Gunkel & Weber (1975)	HWA	T/2	1.018	0.99	(42)	0.89	1.267
Cooper & Wolf (1968)	HWA	T/3	—	0.74	52 to 68	(0.75)	1.054
V.d. Molen & V. Maanen (1978)	LDA	—	—	0.85	45	(0.85)	1.02
Bertrand et al. (1980a)	HFA	T/2	1.11	1.043	45	0.935	(1.4)
Bertrand et al. (1980a)	HFA	T/3	1.11	1.196	42	1.054	(1.5)
Bertrand et al. (1980b)	HFA	T/2	1.11	1.08	45	0.95	(1.44)
Bertrand et al. (1980b)		T/2	1	0.868	—	—	—
Fort & Mala (1982)	Pitot	T/3	—	0.718	—	—	—
Wu & Patterson (1989)	LDA	T/3	1.11	0.745	—	0.663	(0.997)
Costes & Couderc (1982)	HFA	T/2	1.11	0.76	—	0.66	(1.01)
Nouri et al. (1987)	LDA	T/3	1.2	0.822	—	—	—
Mahouast & Cognet (1987)	LDA	T/3	1.03	0.50	—	—	—

*LDA, laser Doppler anemometer HFA, hot film anemometer
HWA, hot wire anemometer Values in ( ) are calculated

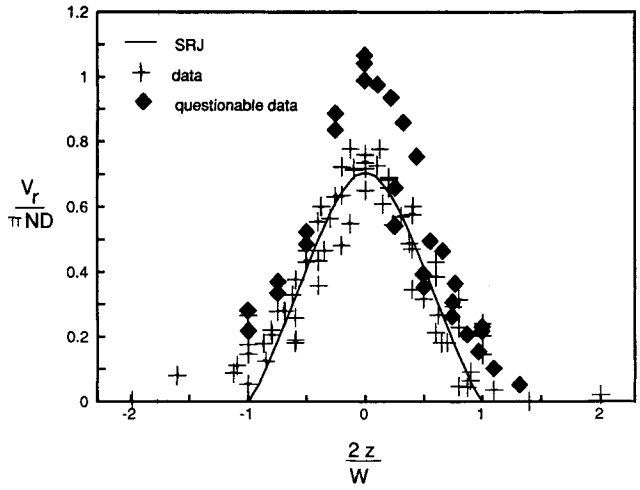

Figure 3. Radial velocity profile at impeller tip

Exp. data points from Wu and Pattersn (1989), Armstrong and Ruszkowski (1988), Wong and Huang (1988), Nouri et al. (1987), Keller (1985), Fort and Mala (1982), Costes and Couderc (1982), Cooper and Wolf (1968)
Questionable data from Gunkel and Weber (1975), Bertrand et al. (1980a,b)

and all of the major experimental techniques. Two sets of data have been classed as questionable; the first is from early laser doppler anemometer (LDA) work (Bertrand et al., 1980a, b), and the second is from an experiment performed in air rather than water (Gunkel and Weber, 1975). The value for which the least information is available, and which is thus the least reliable, is β_o. Again, the median value is used.

It is also possible to predict e from theory, following Eq. 21. J can be simplified to

$$J = 2\lambda\xi^2 q_{M,o}^2 \int_0^1 q'^2 d\eta \tag{30}$$

given the sharp boundaries inherent in the model. Further, the integral can be evaluated numerically, using the values of q' from Table 2, to give

$$\int_0^1 q'^2 d\eta = 0.4167 \tag{31}$$

Given a way to evaluate G, e could be computed using Eq. 21. Kolar et al. (1984) use the same analysis as that applied to centrifugal pumps (McCabe and Smith, 1967) to evaluate the angular momentum integral constraint, Eq. 11. However, this approach requires the assumption of constant velocity profiles in V_r and V_θ across the tip of the impeller blade, which leads to a significant error in the integral of their product. Another approach is to apply a time-averaged macroscopic mechanical energy balance (Bird et al., 1960), which reduces to

$$\left[\frac{1}{2}\frac{\langle V_r^3\rangle}{\langle V_r\rangle}\right]_{\Sigma_V} - \left[\frac{1}{2}\frac{\langle V_z^3\rangle}{\langle V_z\rangle}\right]_{\Sigma_H} + \hat{W} + \hat{E}_v = 0 \tag{32}$$

for the impeller control volume; defined as the volume swept out by the impeller blades. Here Σ_V and Σ_H are the vertical and horizontal surface of this disklike volume.

$\langle V_r^3\rangle$ can be written

$$\langle V_r^3\rangle = \frac{1}{W}\int_{-\frac{W}{2}}^{+\frac{W}{2}} V_r^3 dz = \frac{2}{W}\left(\frac{2\xi_o}{D}\right)^3 (q_{M,o})^3 \frac{W}{2}\int_0^1 q'^3 d\eta \tag{33}$$

the integral

$$\int_0^1 q'^3 d\eta = 0.6881 \tag{34}$$

is calculated numerically from the SRJ similarity profile. From the definition of N_Q,

$$\langle V_r\rangle = \frac{1}{W}\int_{-\frac{W}{2}}^{+\frac{W}{2}} V_r dz = \frac{Q}{\pi DW} = \frac{5N_Q ND^3}{\pi D^2} \tag{35}$$

Taking V_z to be constant over Σ_H, and defined by a material balance around the impeller:

$$\frac{1}{2}\frac{\langle V_z^3\rangle}{\langle V_z\rangle} = \frac{1}{2}V_z^2 = \frac{1}{2}\left(\frac{4ND^3N_Q}{2\pi D^2}\right)^2 \tag{36}$$

By definition,

$$\hat{W} = \frac{-P}{m} = \frac{-N_p\rho N^3 D^5}{\rho N_Q ND^3} \tag{37}$$

$\hat{E}_v$, the dissipation rate within the control volume, is difficult to define or measure. It is dealt with by inserting an efficiency term, η_{eff}, which is the fraction of the power drawn that is not dissipated within the impeller control volume ($\hat{W} + \hat{E}_v = \eta_{eff}\hat{W}$). $q_{M,o}$ will be some fraction of the impeller tip speed: assume this to be one.

Substituting Eqs. 33-37 back into Eq. 32 gives:

$$\left(\frac{\xi_o}{D}\right)^3 = \frac{5}{8\pi^3(0.688)}\left[\frac{2}{\pi}N_p\eta_{eff} + 4\frac{N_Q^3}{\pi^3}\right] \tag{38}$$

for a standard impeller where $W = D/5$. Finally,

$$\frac{e}{D} = \sqrt{\left(\frac{1}{2}\right)^2 - \left(\frac{\xi_o}{D}\right)^2} \tag{39}$$

This shows that e does not depend on N, except possibly through η_{eff}. The only information remaining that is required for the prediction of e is η_{eff}. η_{eff} can be calculated from the results of tank simulations by integrating ϵ over the tank volume. This provides a check on the assumptions used for establishment of the boundary conditions, Eq. 29.

Tank Simulations

Simulations were carried out for two- and three-dimensional cases, using two tank geometries and two finite-difference programs. The system chosen was a standard geometry, with T = 0.456 m, $H = T$, $C = T/2$, $b = T/10$, and the impeller dimensions $D{:}L{:}W$ in the ratio 20:5:4. The impeller speed was

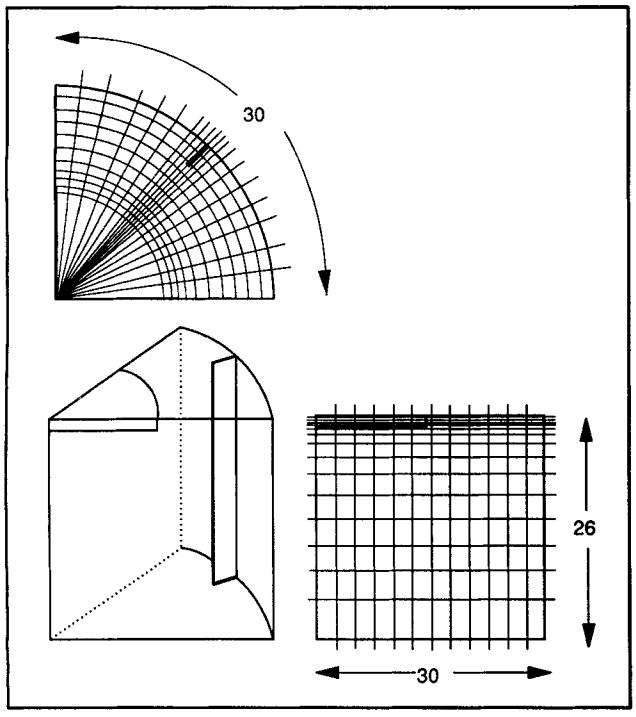

Figure 4. Sketch of calculation domain for three-dimensional finite-difference calculations.

950 rpm, and two impeller diameters were considered: $D = T/2$ and $D = T/3$.

The code used for three-dimensional calculations was FLUENT, a commercial finite-difference package. The calculation domain considered comprised 1/8 of the tank volume. The grid used was $26 \times 30 \times 30$; $z \times r \times \theta$, with domain division for both $D = T/2$ and $D = T/3$ cases as follows:

1. Uniform division of the twenty-eight internal cells in the r direction.

2. In the θ direction, a contraction factor of 0.85 was applied from cells 2–15 where cell 15 is the baffle cell, and an expansion factor of 1.1765 from cells 16–29.

3. In the z direction, uniform division was applied over the extent of the impeller cells 2–7, and an expansion factor of 1.11 was applied over the remaining eighteen cells.

This gave finer definition in the impeller region in the z direction, and refinement around the baffle in the θ direction, as shown in Figure 4.

The boundary conditions were defined as follows:

1. Symmetry at the tank axis, and at the impeller centerline

2. Cyclic, or repeating, at the midbaffle plane; to satisfy a continuous pressure gradient condition

3. No slip at the tank wall, on the baffle, and along the bottom; these boundary conditions were computed using wall functions built into the FLUENT program

4. Vertical impeller boundary, Σ_v, according to the SRJ predictions of q, k, and ϵ, using the recommended experimental values for $q_{M,o}$ and β, Eq. 29.

5. Horizontal impeller boundary (Σ_H) with V_z assumed constant over the impeller: determined from a material balance around the impeller; V_θ taken as solid body rotation; V_r, k, and ϵ set to zero.

Vertical symmetry across the impeller centerline was checked in two dimensions with a free surface at the top of the tank. It was found that deviations from symmetry were slight, and were at their maximum in the center of the tank, a region of minor importance in this flow field.

The normalized residuals of all variables converged to less than 5×10^{-3} within 600 iterations.

Results

The quantity of data acquired from three-dimensional simulations such as these is immense. In this case, each of the 23,400 cells has five values associated with it. Experimental data are not as plentiful, and if attention is confined to comparing the predictions with the data, then evaluation of the model predictions can be reduced to a reasonable task. The region of the tank with the steepest gradients, and the most intense turbulence, is the impeller discharge zone. This is the region of greatest interest for mixing and drop size distribution models, as it is the zone of highest shear. Since the aim of modeling the flow field in the tank is to improve the information available for these models, comparisons of the SRJ predictions with experimental results are concentrated on the impeller discharge zone. The comparisons proceed from the well-established bulk properties of the flow field (flow number, power number, and overall circulation patterns), to quantitative comparisons for which experimental results are fairly plentiful (radial decay of V_r, k, and ϵ), to details of the flow field for which data are scarce (profiles of k and V_r, behavior of the vortex behind the baffle). Given the excellent agreement of the model predictions with all of these experimental criteria, the SRJ model results are used to provide additional information about the flow field, in the form of average values of ϵ.

Dimensionless numbers

Two dimensionless numbers, N_p and N_Q, are well established for the Rushton turbine. The flow number (Revil, 1982), has been defined, and set to a value of approximately 0.75. Integration of the radial velocity profile predicted by the SRJ model at the tip of the impeller gives $N_Q = 0.78$, a difference of 4%. The power number is usually reported (Bates et al., 1963; Nienow and Miles, 1971) as 5.0, although there is significant experimental deviation in this number. Bujalski et al. (1987) did a careful study of the power number and found that for high Reynolds numbers, variations in N_p arose from changes in the disk thickness, as compared to the impeller diameter, and changes in scale. N_p was independent of D/T.

The mechanical energy balance discussed previously can be used to calculate the fraction of the power dissipated in the tank, η_{eff}. Substituting the established experimental values $N_p = 5.0$, $N_Q = 0.75$, and $\beta = 45°$ into Eq. 38 given $\eta_{eff} = 0.46$. An independent estimate of η_{eff} can be computed by integrating the dissipation rate of each computational cell over the free volume of the tank. If the integral

$$\frac{\rho \int \epsilon dV}{\rho N^3 D^5} = \eta_{eff} N_P \tag{40}$$

is computed from the three-dimensional simulation results, the prediction of η_{eff} is 0.46 for $D = T/2$ and 0.56 for $D = T/3$

where $N_p = 5.0$ has been used in both cases. This means that approximately 50% of the energy is dissipated before the fluid reaches the impeller periphery. A similar fraction of energy dissipation in the impeller control volume (50%) is reported by Placek and Tavlaride (1982). A similar trend of increasing η_{eff} with decreasing D/T was reported by Placek and Tavlarides (1986).

Equations 38 and 40 are also used to check the assumption of constant β_o, made in order to establish the boundary conditions. If N_p and N_Q are constant, and computational results show that η_{eff} varies with D/T, then β_o cannot be constant. If β_o is calculated based on the computational results, $\beta_o = 44.9°$ for $D = T/2$ and $\beta_o = 39.7°$ for $D = T/3$. Examination of available experimental results, Table 3, shows that this variation is very small compared to that seen in experiments. Given the excellent agreement of model results with experiment, even using the assumption of constant β_o, and the lack of reliable experimental evidence for a better evaluation, it seems best to accept this approach. The variation in η_{eff} appears to be related to the changing tank geometry. The implications of this are discussed further in the later section on average values.

Comparing the SRJ results to those given by other authors shows an unprecedented emphasis on the impeller stream. If considered in terms of the total power, these results can be stated as 54% dissipated inside the impeller, 35% in the impeller stream, and 11% in the bulk of the tank, or the circulation zone. Cutter (1966) suggests only 20% dissipation in the impeller, 50% in the impeller stream, and 20–40% in the bulk of the tank. Gunkel and Weber (1975) state that 38% of the energy is dissipated inside the impeller boundaries. Okamoto et al. (1981) find that none of the energy is dissipated inside the impeller. Wu and Patterson (1989) state that 30% of the energy is dissipated in the impeller, 30% in the impeller stream, and 40% in the bulk of the tank. A reported experimental uncertainty of ± 15% brings these measurements into the range of the SRJ model predictions.

Mean velocity fields

The flow pattern in a stirred tank with a radial impeller is known to consist of two toroidal vortices or circulation loops, one above and one below the impeller, which rotate such that the impeller stream is radially directed outward. This was observed in the results of the simulations and has been reported in detail elsewhere (Costes and Couderc, 1988; Yianneskis et al., 1987). In the $r = \theta$ planes, it has been reported that there is a vortex behind the baffles. Flow visualization experiments show that this vortex persists only in the vicinity of the impeller plane, and decays rapidly with increasing or decreasing z. This was also shown in the results of the simulations, as illustrated in Figure 5.

The decay of V_r on the impeller centerline at the midbaffle plane for $D = T/3$ is shown in Figure 6. Since all available experimental results are for $D = T/3$, the computed decay for $D = T/2$ is not shown. The similarity solution predicts decay of $V_{r,m}$ with ξ^{-1}, which is not the case for the outer region of the tank. This is due to the influence of the baffle.

Figure 7 shows the computed profile of V_r at $2r/D = 1.5$ for $D = T/3$. All of the experimental profiles shown in this figure are for cases where the impeller was set at a clearance of $C = T/3$. Because of this asymmetry, the experimental

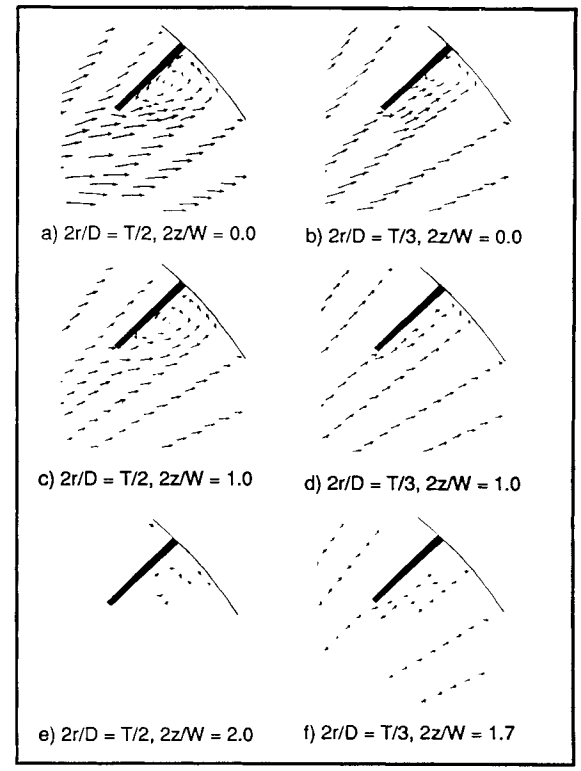

Figure 5. Axial variation in velocity field showing baffle vortex decay.

velocity profiles are skewed to one side. They are also more elongated than the computed profile. Given the uncertainty in comparing asymmetric data to a symmetric case, agreement between experimental and computational results is good.

Two-dimensional vs. three-dimensional

Figure 8 gives an example of the three-dimensional character of the flow field in the outer 25% of the tank. The decay of k is virtually independent of angular position, from 4 degrees behind the baffle to 3.5 degrees ahead of the baffle. In the

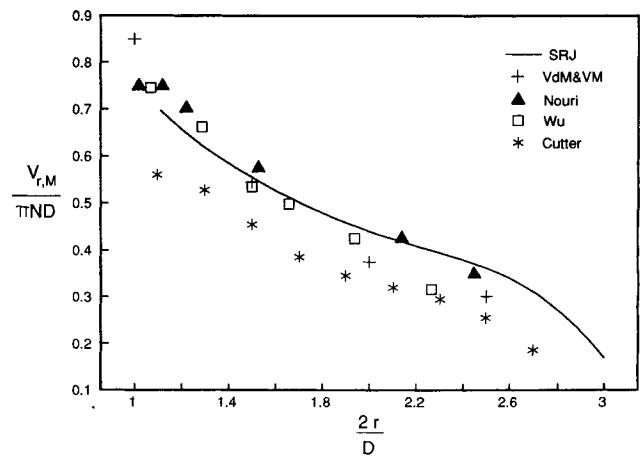

Figure 6. Decay of V_r on impeller centerline for $D = T/3$.

SRJ and Nouri results at 45° plane; other angular positions not reported

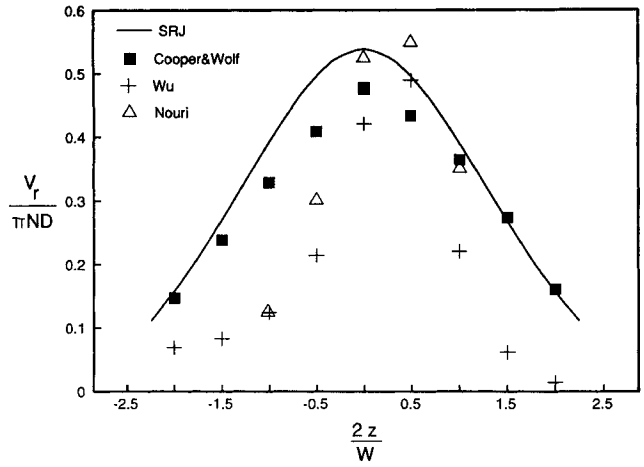

Figure 7. Profile of radial component of velocity at $2r/D = 1.5$.

SRJ and Cooper and Wolf use a clearance of $T/2$; Wu and Nouri are at $C = T/3$.
Angular position 45° for SRJ and Nouri, not reported for other data

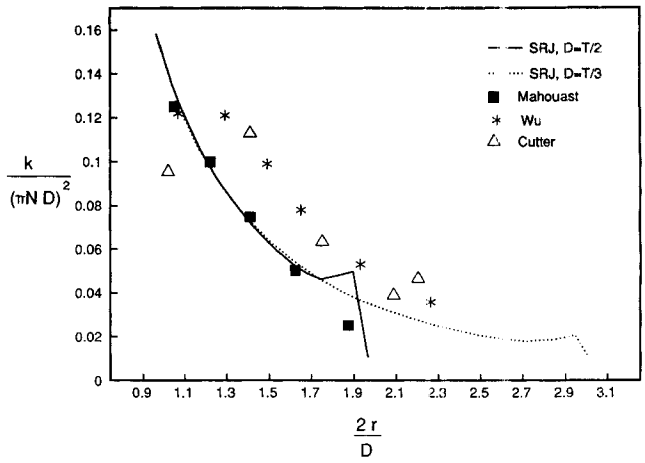

Figure 9. Decay of dimensionless turbulence kinetic energy on impeller centerline: comparison with experimental results.

SRJ and Mahouast at 45° plane; Wu and Cutter do not report angular position

baffle zone, however, changes are rapid and extreme. Out to a radial position of $2r/D \approx 1.48$, the effects of the baffle are negligible, for the $D = T/2$ case. This lends credence to the assumption of axisymmetric flow at the impeller periphery, while showing the importance of an accurate representation of this complex geometry.

Turbulence kinetic energy, k

The decay of k on the impeller centerline at the midbaffle plane is shown in Figure 9 for both impeller diameters and three sets of experimental data. Only those values of k that include all three components of the velocity fluctuation are considered; those that ignore v_θ' ignore the second largest component of k and are thus subject to severe underprediction. Mahouast et al. (1989) and Wu and Patterson (1989) report measurements taken using laser Doppler anemometer. Cutter's (1966) data were obtained by use of a photographic technique. Agreement between the model predictions and the experimental results is very good. The turbulence kinetic energy, made dimensionless with V_{TIP}, is shown to scale exactly with $2r/D$.

The profiles of k across the impeller tip at three radial positions are shown in Figure 10. It appears that the curvature in the model is more extreme that that seen in experiments, but that the spreading and decay are fairly well predicted. Agreement down to this level of detail in the flow field has not previously been reported.

Turbulence kinetic energy dissipation rate ϵ

The decay of ϵ on the impeller centerline at the midbaffle plane is shown in Figure 11 for both impeller diameters and five sets of experimental data. The radial decay of ϵ closely

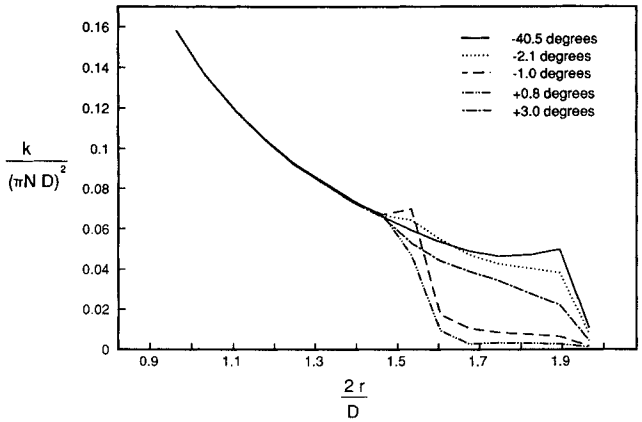

Figure 8. Angular variation in centerline decay of dimensionless turbulence kinetic energy as predicted by SRJ simulations ($D = T/2$)

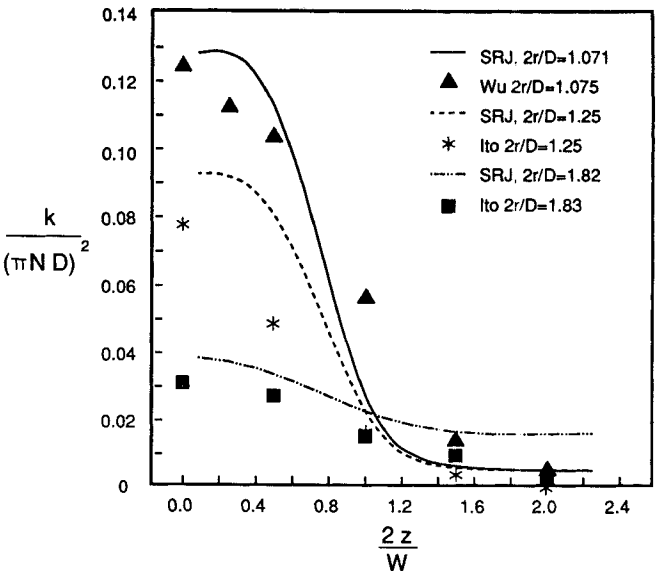

Figure 10. Profiles of turbulence kinetic energy in impeller stream at various radial positions.

SRJ results at midbaffle plane (45°); results by Ito at 45°, Wu at 30°

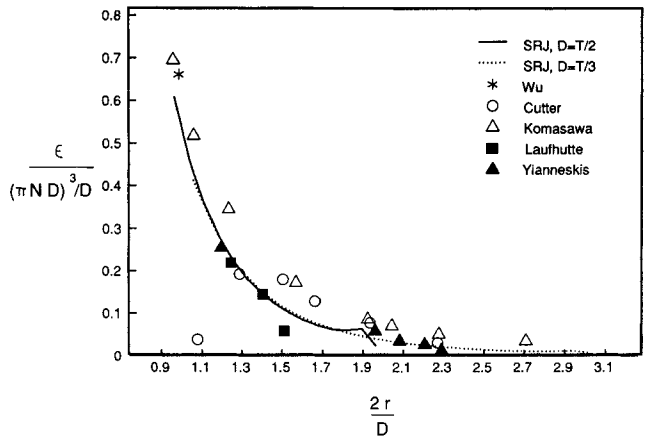

Figure 11. Decay of ϵ on impeller centerline: comparison with experimental results.

SRJ results on midbaffle (45°); data by Wu at 30°, Komasawa at 22.5°; Laufhutte at 0°. Cutter and Yianneskis do not report angular position

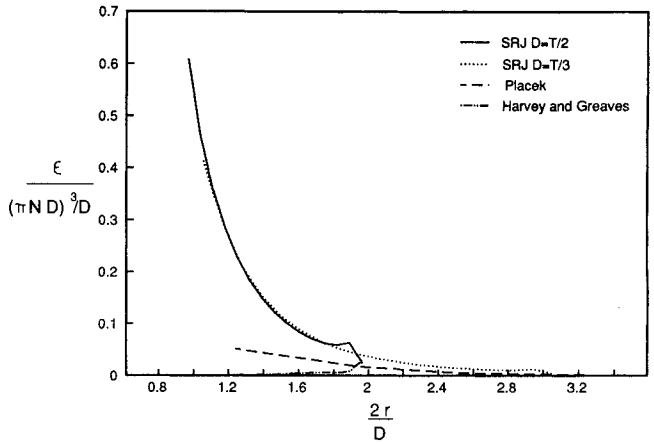

Figure 12. Comparison of various model predictions of decay of ϵ on impeller centerline.

SRJ results on midbaffle (45°) plane; other models used a two-dimensional calculation

follows several previously reported experimental studies. The degree of agreement shown here, especially in the immediate vicinity of the impeller, indicates that the SRJ model accurately describes the impeller boundary condition.

Previous authors (Wu and Patterson, 1989, Laufhutte and Mersmann, 1987) have reported surveys of ϵ data that showed wide variations in the results. The primary cause of this apparent deviation is not, as was suggested, the experimental technique or evaluation theory used, but incorrect scaling of ϵ. The general practice has been to plot $\epsilon/\bar{\epsilon}$ vs. $2r/D$, where $\bar{\epsilon}$ is the power input per unit mass. Use of $\bar{\epsilon}$, although appealing from a design point of view, contaminates the data with introduction of the tank diameter, cubed. If the scaling suggested by the more theoretically rigorous similarity solution is used, the data collapse very nicely, as shown in Figure 11. This new scaling divides the value of ϵ by V^3_{TIP}/D. Use of this modified dimensionless variable allows exact scale-up, over the axisymmetric region, from $D = T/2$ to $D = T/3$.

Comparison of the SRJ model predictions with other model predictions is shown in Figure 12. Harvey and Greaves (1982) set k and ϵ equal to zero at the impeller boundary. Their predictions of ϵ are not only low but show an incorrect trend, increasing as the wall is approached. Placek and Tavlarides' (1986) model gives very low predictions close to the impeller, but approaches experimental results in outer regions. Their calculations concentrated on a case where $D = T/4$, so the effects of this underprediction close to the impeller were minimized. The SRJ model correctly predicts the exponential rise of ϵ as the impeller is approached. No other model is close to the data in this region.

Average values

For the purposes of further modeling of reactor and chemical processes where computation of the detailed fluid mechanics is not practical due to the large number of variables involved, it is useful to define zones in the stirred tank where average values of the turbulence quantities may be applied. Based on the results of these simulations, two zones have been defined. The first is the impeller discharge zone. This zone extends over the region where the SRJ dominates, and the effects of the baffles are not felt. The value of ϵ_{ave} for this zone is virtually independent of D/T. The second zone comprises the remaining free volume of the tank, and reflects the influence of changing D/T. More detailed zones (e.g., a baffle zone) could not be defined because of the changing geometry. While the impeller zone does not "see" its surroundings, the geometry has significant effects outside this zone. Of the total power drawn (calculated from N_p), approximately 50% is dissipated within the impeller control volume. The volume-averaged, dimensionless dissipation rate is constant with varying D/T within the impeller discharge zone (defined using dimensionless coordinates). The power remaining is dissipated in the bulk of the tank. This means that the bulk value can be expected to vary, depending on the tank geometry, especially D/T.

In order to define these zones rigorously, the dimensionless, volume-averaged ϵ is defined as:

$$\epsilon_{ave} = \frac{\int \epsilon dV}{\frac{(\pi ND)^3}{D}\int dV} \tag{41}$$

This was computed for each of the r, z, and θ planes so that the variation of ϵ_{ave} could be examined and appropriate zones chosen. Most of the variation occurs in the immediate vicinity of the impeller, from $2z/W = 0$ to 1.0 (ϵ_{ave} decays to 10% of its initial value), and $2r/D = 1$ to 1.45 (ϵ_{ave} decays to 30% of the boundary value). The limiting value of $2r/D$ must be chosen with some care if ϵ_{ave} for the impeller discharge zone is to remain constant from $D = T/2$ to $D = T/3$: the zone cannot extend into the region where the influence of the baffles begins to be felt; see Figure 8. For the limits given above, $\epsilon_{ave} = 0.195$ for $D = T/2$ and $\epsilon_{ave} = 0.192$ for $D = T/3$, a difference of 1.6%.

The only variation in ϵ_{ave} not covered by the impeller discharge zone is that due to the influence of the baffles. This variation is shown for both cases in Figure 13. Note that while the trends are clearly analogous for the two cases, no way of scaling the results so that they collapse onto one curve was

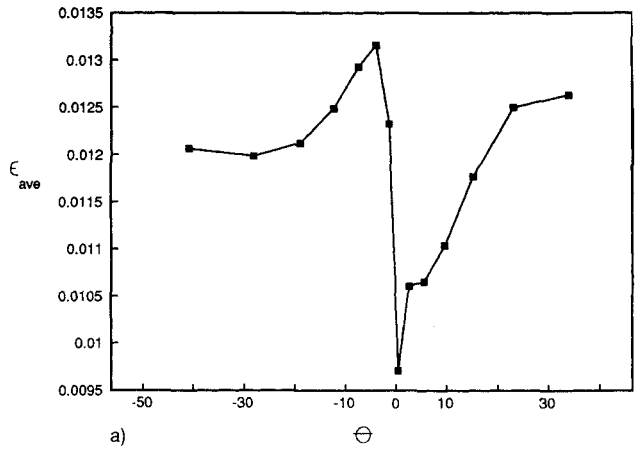

a. $D = T/2$

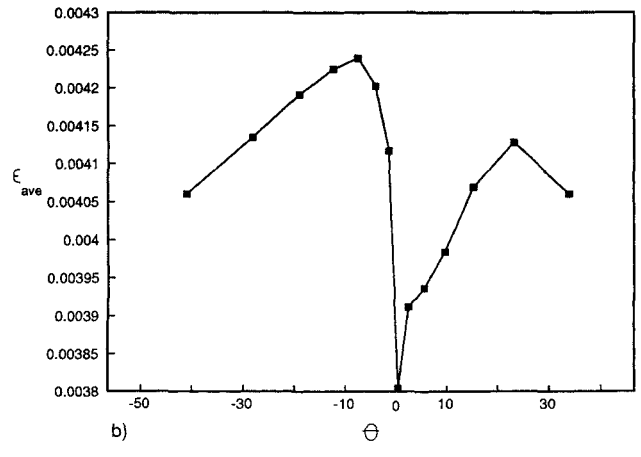

b. $D = T/3$

Figure 13. Variation of ϵ_{ave} with θ.

found. It was concluded that this is mainly because the power input, and therefore the energy available to be dissipated, is dependent only on the impeller diameter and rotational speed; a smaller impeller in the same size tank (with constant N) has much less power available to be dissipated in the bulk of the tank. The volume of the tank relative to the volume of the impeller is much larger. Because any value of ϵ_{ave} defined for this zone would only be applicable to a specific case, no baffle zone has been defined.

For the bulk of the tank, ϵ_{ave} is 5.59×10^{-3} for $D = T/2$, and 2.07×10^{-3} for $D = T/3$. The volume covered by these averages is the free volume in the tank not included in the impeller zone. The baffle variations have been lumped into these averages.

Conclusions

The turbulent swirling radial jet model can successfully be applied to the modeling of flow in stirred tanks with radial impellers, specifically the Rushton turbine. This model has been extended from the case of closure using the mixing length hypothesis, to closure using the $k-\epsilon$ model. In addition, the model parameters have been clarified so that they have clear physical meaning. The success of this modeling effort indicates that the modified $k-\epsilon$ models recently proposed by several authors are not necessary, provided the proper boundary conditions are applied when using the standard $k-\epsilon$ model.

The most reliable way to treat the drag introduced by the baffles around the tank periphery is to specify them as part of a three-dimensional computational geometry. This allows elimination of the pressure-induced drag term, which is in essence of tuning parameter, so that the flow field can be calculated with much less *a priori* knowledge of the result.

Three-dimensional simulations based on these principles yielded excellent agreement with experimental results. Details of the velocity field, decay of k and ϵ on the impeller centerline, profiles of V_r and k at various radial positions, and the total power dissipated were all accurately predicted. In contrast, previous studies have concentrated on predictions of the mean velocity field, and have shown only qualitative agreement with the turbulence quantities k and ϵ.

Appropriate zones were recommended for use in modeling efforts where the main interest is not the detailed fluid mechanics, but other processes such as mixing or reaction. Average values of ϵ were presented for these zones.

Acknowledgment

The initial two-dimensional calculations were performed by C. P. Chen. S. Kresta was funded by a National Science and Engineering Research Council of Canada (NSERC) postgraduate scholarship during this study. The financial support of this research by NSREC is gratefully acknowledged.

Notation

b = baffle width = $T/10$
B = holding variable
C = impeller clearance = $T/2$
C_{ϵ_1} = $k-\epsilon$ model constant
C_{ϵ_2} = $k-\epsilon$ model constant
C_μ = $k-\epsilon$ model constant
D = impeller diameter
e = radius of cylinder, centered at $r = 0$, which defines the origin of the system tangential half-planes
$\hat{E}_v$ = rate at which system loses energy through dissipation, per unit mass
$f(\eta), g(\eta), p(\eta), m(\eta)$ = similarity variables
G = total radial flux of angular momentum, or moment of momentum
H = height of liquid in tank = T
J = total ξ flux of ξ momentum
k = turbulence kinetic energy per unit mass, m^2/s^2
k_p = turbulence kinetic energy of large-scale vortices (Placek and Tavlarides, 1985)
L = length of impeller blades = $D/4$
m = mass rate of flow through impeller
M_∞ = total radial flux of radial momentum at infinity
N = rotational speed of impeller, rps
N_p = power number = $P/(\rho N^3 D^5)$
N_Q = flow number = $Q/(ND^3)$
P = power input
q = component of velocity in ξ direction
q' = q/q_M = dimensionless q velocity determined from similarity solution
q_M = centerline q velocity
$q_{M,o}$ = centerline q velocity at impeller periphery
Q = primary flow
r = radial coordinate, origin at center of impeller
T = tank diameter
v_r' = turbulent velocity fluctuation of r component of velocity

V_r = component of velocity in r direction
V_{TIP} = impeller tip speed = πND
v'_θ = turbulent velocity fluctuation of θ component of velocity
V_θ = component of velocity in θ direction
v'_z = turbulent velocity fluctuation of z component of velocity
V_z = component of velocity in z direction
W = width of impeller blade = $D/5$
$\hat{W}$ = rate at which system performs mechanical work on surroundings, per unit mass
z = axial coordinate, origin at center of impeller

Greek letters

β = angle of declination of flow
β_o = β at impeller periphery
γ = constant
$\delta(\xi)$ = jet width
δ_o = jet width at impeller periphery
ϵ = turbulence kinetic energy dissipation rate, m^2/s^3
$\bar{\epsilon}$ = power input per unit mass
ϵ_{ave} = volume-averaged ϵ
η = similarity coordinate
η_{eff} = impeller efficiency
θ = angular coordinate, origin at baffle plane
λ = jet spreading rate = constant = eigenvalue
ν_t = turbulent viscosity
ξ = coordinate in direction of flow, see Figure 1
ξ_o = value of ξ at impeller periphery
ξ_v = "virtual" origin of SRJ, Figure 2
ρ = fluid density, kg/m^3
σ_k = $k-\epsilon$ model constant
σ_ϵ = $k-\epsilon$ model constant
Σ_H = horizontal impeller boundary
Σ_V = vertical impeller boundary
τ = shear stress, rz, θz, or ξz
Ψ = stream function

Other symbols

$\langle\rangle$ = quantity averaged over a surface

Literature Cited

Amstrong, S. G., and S. Ruszkowski, "The Flow Field in the Discharge Stream of Disk Turbines," *Proc. 6th Eur. Conf. on Mixing, Pavia, Italy*, BHRA Fluid Eng. Cntr., Springer, 1 (1988).

Bates, R. L., P. L. Fondy, and R. R. Corpstein, "An Examination of Some Geometric Parameters of Impeller Power," *Ind. Eng. Chem. Process Des. Dev.*, **2**, 311 (1963).

Bertrand, J., J. P. Couderc, and H. Angelino, "Power Consumption, Pumping Capacity, and Turbulence Intensity in Baffled Stirred Tanks: Comparison Between Several Turbines," *Chem. Eng. Sci.*, **35**, 2157 (1980a).

Bertrand, J., J. P. Couderc, and H. Angelino, "Ecoulement dans le Courant de Refoulement d'une Turbine a Disque et Six Pales Plates Dans une Cuve Munie de Chicanes," *Chem. Eng. J.*, **19**, 113 (1980b).

Bird, R. B., W. E. Stewart, and E. N. Lightfoot, *Transport Phenomena*, Wiley, Toronto (1960).

Bujalski, W., A. W. Nienow, S. Chatwin, and M. Cooke, "The Dependency on Scale of Power Numbers of Rushton Disc Turbines," *Chem. Eng. Sci.*, **42**, 317 (1987).

Chen, C. P., and P. E. Wood, "Numerical Modeling of the Turbulent Flow in a Stirred Tank," *79th AIChE Meeting*, Miami Beach (1988).

Cooper, R. G., and D. Wolf, "Velocity Profiles and Pumping Capacities for Turbine-Type Impellers," *Can. J. Chem. Eng.*, **46**, 94 (1968).

Costes, J., and J. P. Couderc, "Pumping Capacity and Turbulence Intensity in Baffled Stirred Tanks: Influence of the Size of the Pilot Unit," *4th Euro. Conf. on Mixing*, Leewenhorst (1982).

Costes, J., and J. P. Couderc, "Study by Laser Doppler Anemometry of the Turbulent Flow Induced by a Rushton Turbine in a Stirred Tank: Influence of the Size of the Units. I: Mean Flow and Turbulence," *Chem. Eng. Sci.*, **43**, 2751 (1988).

Cutter, Louis A., "Flow and Turbulence in a Stirred Tank," *AIChE J.*, **12**, 35 (1966).

DeSouza, A., and R. W. Pike, "Fluid Dynamics and Flow Patterns in Stirred Tanks with a Turbine Impeller," *Can. J. Chem. Eng.*, **50** (1972).

Fort, I., and J. Mala, "Hydraulic Characteristics of Turbine Impeller," *Coll. Czech. Chem. Comm.*, **47**, 421 (1982).

Gunkel, A. A., and M. E. Weber, "Flow Phenomena in Stirred Tanks. 1: The Impeller Stream," *AIChE J.*, **21**, 931 (1975).

Harvey, P. S., and M. Greaves, "Turbulent Flow in an Agitated Vessel, I: A Predictive Model," *Trans. Inst. Chem. Eng.*, **60**, 195 (1982).

Harvey, P. S., and M. Greaves, "Turbulent Flow in an Agitated Vessel, II: Numerical Solution and Model Predictions," *Trans. Inst. Chem. Eng.*, **60**, 201 (1982).

Hutchings, B. J., R. J. Weetman, and B. R. Patel, "Computation of Flow Fields in Mixing Tanks with Experimental Verification," paper TN-481, *ASME Meeting*, San Francisco (1989).

Ito, S., H. Ogawa, and N. Yoshida, "Turbulence in Impeller Stream in a Stirred Vessel," *J. Chem. Eng. Japan*, **8**, 206 (1975).

Ju, S. Y., T. M. Mulvahill, and R. W. Pike, "Turbulent, Three-Dimensional Velocity Profiles in a Turbine-Stirred Vessel," *Mixing XI—Eng. Found. Conf. on Mixing*, Heniker, NH (1987).

Ju, S. Y., T. M. Mulvahill, and R. W. Pike, "Three-Dimensional Turbulent Flow in Agitated Vessels with a Nonisotropic Viscosity Turbulence Model," *Can. J. Chem. Eng.*, **68**, 3 (1990).

Kaminoyama, M., F. Saito, and M. Kamiwano, "Numerical Analysis of Three-Dimensional Flow Behavior of Pseudoplastic Liquid in a Stirred Vessel with Turbine Impellers," *Kag. Kog., Ron.*, **14**, (6) 786 (1988).

Keller, D. B. A., "To Determine the Pumping Capacity of a Disk Turbine Impeller at Different Reynolds Numbers," *5th Eur. Conf. on Mixing*, Wurtzberg, Germany (1985).

Kolar, V., P. Filip, and A. G. Curev, "The Swirling Radial Jet," *Appl. Sci. Res.*, **39**, 329 (1982).

Kolar, V., P. Filip, and A. G. Curev, "Hydrodynamics of a Radially Discharging Impeller Stream in Agitated Vessels," *Chem. Eng. Comm.*, **27**, 313 (1984).

Komasawa, I., R. Kuboi and T. Otake, "Fluid and Particle Motion in Turbulent Dispersion: I: Measurement of Turbulence of Liquid by Continual Pursuit of Tracer Particle Motion," *Chem. Eng. Sci.*, **29**, 641 (1974).

Laufhutte, H. D. and A. Mersmann, "Local Energy Dissipation in Agitated Turbulent Fluids and Its Significance for the Design of Stirring Equipment," *Chem. Eng. Technol.*, **10**, 56 (1987).

Launder, B. E., and D. B. Spalding, *Mathematical Models of Turbulence*, Academic Press, London (1972).

Mahouast, M., and G. Cognet, "Analysis of Turbulent Mixing in a CFSTR from LDV Measurements," *ASME 3rd Int. Symp. on Laser Anemometry*, ASME, FED, **55**, 157 Boston (1987).

Mahouast, M., G. Cognet, and R. David, "Two-Component LDV Measurements in a Stirred Tank," *AIChE J.*, **35**, 1770 (1989).

McCabe, W. L., and J. C. Smith, *Unit Operations of Chemical Engineering*, 2d ed., McGraw-Hill, Toronto (1967).

Middleton, J. C., F. Pierce, and P. M. Lynch, "Computations of Flow Fields and Complex Reaction Yield in Turbulent Stirred Reactors, and Comparison with Experimental Data," *Chem. Eng. Res. Des.*, **64** 18 (1986).

Nienow, A. W., and D. Miles, "Impeller Power Numbers in Closed Vessels," *Ind. Eng. Chem. Process Des. Dev.*, **10**, 41 (1971).

Nouri, J. M., J. H. Whitelaw, and M. Yianneskis, "The Scaling of the Flow Field with Impeller Size and Rotational Speed in a Stirred Reactor," *2nd Int. Conf. on Laser Anemometry—Advances and Applications*, Strathclyde, UK (1987).

Obeid, A., I. Fort, and J. Bertrand, "Hydrodynamic Characteristics of Flow in Systems with Turbine Impellers, LXI: Studies in Mixing," *Coll. Czech. Chem. Comm.*, **48**, 568 (1982).

Okamoto, Y., N. Nishikawa, and K. Hashimoto, "Energy Dissipation Rate Distribution in Mixing Vessels and Its Effects on Liquid–Liquid Dispersion and Solid–Liquid Mass Transfer," *Int. Chem. Eng.*, **21**, 88 (1981).

Pericleous, K. A., and M. K. Patel, "The Source-Sink Approach in the Modeling of Stirred Reactors," *Phys. Chem. Hydrodynam.*, **9** 279 (1987).

Placek, J., and L. L. Tavlarides, "A Turbulent Flow Model Applied to Fluid Flow in a Stirred Tank," paper 101c, *AIChE meet.*, Los Angeles (1982).
Placek, J., and L. L. Tavlarides, "Turbulent Flow in Stirred Tanks, I: Turbulent Flow in the Turbine Impeller Region," *AIChE J.*, **31**, 1113 (1985).
Placek, J., L. L. Tavlarides, G. W. Smith, and I. Fort, "Turbulent Flow in Stirred Tanks, II: A Two-Scale Model of Turbulence," *AIChE J.*, **32**, 1771 (1986).
Ramos, J. I., "Turbulent Nonreacting Swirling Flows," *AIAA J.*, **22**, 846 (1984).
Ranade, V. V., and J. B. Joshi, "Flow Generated by Pitched-Blade Turbines. I: Measurements Using Laser Doppler Anemometer," *Chem. Eng. Comm.*, **81**, 197 (1989).
Ranade, V. V., J. B. Joshi, and A. G. Marathe, "Flow Generated by Pitched-Blade Turbines. II: Simulation using $k-\epsilon$ model," *Chem. Eng. Comm.*, **81**, 225 (1989).
Revill, B. K., "Pumping Capacity of Disc Turbine Agitators—a Literature Review," *4th Eur. Conf. on Mixing*, Leewenhorst (1982).
Riley, N., "Radial Jets with Swirl. 1: Incompressible Flow," *Q. J. Mech. Applied Math*, **15**, 435 (1962).
Stoots, C. M., and R. V. Calabrese, "The Trailing Vortex System Behind a Rushton Turbine Blade," *Mixing XIII—Eng. Found. Conf. on Mixing.*, (1989).
Van der Molen, K., and H. R. E. Van Maanen, "Laser Doppler Measurements of the Turbulent Flow in Stirred Vessels to Establish Scaling Rules," *Chem. Eng. Sci.*, **33** 1161 (1978).
Van't Riet, K., and J. M. Smith, "The Trailing Vortex System Produced by Rushton Turbine Agitators," *Chem. Eng. Sci.*, **30**, 1093 (1975).
Wong, C. W. and C. T. Huang, "Flow Characteristics and Mechanical Efficiency in Baffled Stirred Tanks with Turbine Impellers," *Proc. 6th Eur. Conf. on Mixing*, Pavia, Italy, BHRA Fluid Eng. Cntr., Springer (1988).
Wood, P. E., "Studies of Mean Reynolds Stress Turbulence Models of Turbulent Flow," PhD Thesis, Calif. Inst. Technol. (1978).
Wood, P. E., and C. P. Chen, "Turbulence Model Predictions of the Radial Jet—A Comparison of $k-\epsilon$ Models," *Can. J. Chem. Eng.*, **63** 177 (1985).
Wu, H., and G. K. Patterson, "Laser Doppler Measurements of Turbulent Flow Parameters in a Stirred Mixer," *Chem. Eng. Sci.*, **44**, 2207 (1989).
Yianneskis, M., Z. Popiolek, and J. H. Whitelaw, "An Experimental Study of the Steady and Unsteady Flow Characteristics of Stirred Reactors," *J. Fluid Mech.*, **175**, 537 (1987).

Manuscript received Mar. 26, 1990, and revision received Jan. 17, 1991.